Environmental Science
Processes & Impacts

Emerging investigator series: Spatial distribution of dissolved organic matter in ice and at air-ice interfaces

Journal:	*Environmental Science: Processes & Impacts*
Manuscript ID	EM-ART-04-2019-000190.R1
Article Type:	Paper
Date Submitted by the Author:	13-Jun-2019
Complete List of Authors:	Chakraborty, Subha; University of Saskatchewan, Chemistry Kahan, Tara; University of Saskatchewan, Chemistry

Organic matter is a common component of environmental snow and ice. A few studies have shown that it can greatly affect reactivity there, for example by acting as a photosensitizer or by creating nonpolar micro-environments. We used Raman microscopy to investigate the distribution of three types of organic matter within ice and at air-ice interfaces. Our results show that different types of organic matter have different distributions and local concentrations at air-ice interfaces, as well as different effects on the underlying ice surface. Different types of organic matter may therefore have very different effects on reaction rates at air-ice interfaces.

Emerging investigator series: Spatial distribution of dissolved organic matter in ice and at air-ice interfaces

Subha Chakraborty[1,2] and Tara F. Kahan[1,2*]

1. Department of Chemistry, University of Saskatchewan, 110 Science Place, Saskatoon, SK 37N 5C9, Canada
2. Department of Chemistry, Syracuse University, 1-014 Center for Science and Technology, Syracuse, NY 13244, USA

*Author to whom correspondence should be addressed: tara.kahan@usask.ca, Ph: +1 (306) 966-1168.

Abstract:

Dissolved organic matter (DOM) is a common solute in snow and ice at Earth's surface. Its effects on reaction kinetics in ice and at air-ice interfaces can be large, but are currently difficult to quantify. We used Raman microscopy to characterize the surface and bulk of frozen aqueous solutions containing humic acid, sodium dodecyl sulfate (SDS), and citric acid at a range of concentrations and temperatures. The surface-active species (humic acid and SDS) were distributed differently than citric acid. Humic acid and SDS are almost completely excluded to the air-ice interface during freezing, where they form a film that coats the surface nearly completely. A liquid layer that coats the entire surface was observed at all humic acid and SDS concentrations. Citric acid, which is smaller and less surface active, is excluded to liquid channels at the air-ice interface and within the ice bulk, as has previously been reported for ionic solutes such as sodium chloride. Incomplete surface wetting was observed at all citric acid concentrations and at all temperatures (up to −5 °C). Citric acid appears to be solvated in frozen samples, but SDS and humic acid do not. These results will improve our understanding of the effects of organic solutes on environmental and atmospheric chemistry within ice and at air-ice interfaces.

Keywords: Dissolved organic carbon (DOC), surfactant, quasi-liquid layer, freeze exclusion, cryosphere, spectroscopy

Introduction

Ice surfaces have long been recognized as important environmental reaction media.[1, 2] Kinetics of several atmospherically-relevant photolytic[3-12] and heterogeneous[5, 13-17] reactions have been reported to be very different at ice surfaces than in liquid water or at liquid water surfaces. Solutes in water are generally excluded from the ice matrix upon freezing due to strong, directional hydrogen bonding in water. Different solutes, upon freezing, experience different degrees of exclusion and modify the surface properties of the

frozen solution accordingly. Several studies have reported the effects of environmentally-relevant ionic and small organic solute impurities on the surficial properties of ice.[18-27] Ionic impurities, for example, are known to increase the activity and water fraction on the surface of frozen solutions, as verified by theoretical[19, 20] and experimental[27-30] studies. Several ionic solutes are known to form deep channels or isolated patches of concentrated liquid brine on the ice-surface.[22-25, 31] Our previous study showed, for example, formation of 10's of μm deep and 5 – 20 μm wide brine-channels in frozen seawater and aqueous 0.6 M sodium chloride (NaCl) solutions.[23] Freeze exclusion of ionic species appears to lead to liquid water that is distributed throughout the ice sample, including at the air-ice interface. The resultant changes in local solute concentration and fractional surface liquid coverage can affect reaction kinetics at ice surfaces.[11] To quantitatively predict the effects of solutes on chemistry at air-ice interfaces, the distribution of solutes and of liquid water must be known, but to date they often are not.

Most studies that have investigated the effects of solutes on properties of air-ice interfaces have focused on inorganic ionic species. Organic matter (OM) is a common solute in ice. In liquid atmospheric aqueous phases it can greatly impact gas-surface partitioning and reaction kinetics by forming films at the interface.[32-36] Organic matter has been reported to suppress photolysis of some pollutants in ice and at ice surfaces by reducing local polarity[9] and via competitive photon absorption (the "inner filter effect"),[10] and to enhance photolysis of other pollutants via production of reactive oxygen species.[37, 38] Irradiation of OM-containing snow and ice has been reported to release gas-phase products including formaldehyde, acetone, and nitrous acid.[39, 40] A few studies have reported distributions of OM within and at the surface of ice samples. Some fluorescent dyes have been suggested to reside within liquid compartments inside of ice,[41-43] and molecular dynamics (MD) simulations suggest that organic molecules such as octanol and octanal form films at ice surfaces,[25] while glyoxal forms heterogeneous clusters at ice surfaces.[18] The distributions of common environmental OM such as fulvic and humic acids in ice have not been reported. We used Raman spectroscopy and mapping to probe the surface and sub-surface presence of three organic solutes in frozen aqueous solutions. We report the distributions of humic acid, sodium dodecyl sulfate (SDS), and citric acid across the ice surface and throughout the bulk of the sample, and investigate their effects on the liquid water fraction of the ice. Our results may improve our ability to model chemistry in organic-containing snow and ice.

Materials and methods

***Sample preparation*:**

Solid humic acid (HA, International Humic Substances Society), sodium dodecyl sulfate (SDS, Sigma-Aldrich, ≥ 98.5%), or citric acid (CA, Sigma-Aldrich, ≥ 99.5%) was dissolved in deionized (DI) water of resistivity 18.2 MΩ.cm. The concentrations used are shown in Table 1.

Table 1: Solute concentrations in liquid and frozen samples

	Concentration (g/L)	
Sample	**Liquid**	**Ice[a]**
Suwannee River humic acid (HA) Std. III	$1\times 10^{-3} - 3\times10^{-2}$	$3\times10^{-6} - 3\times10^{-2}$
Sodium dodecyl sulphate (SDS)	1 – 200	1 – 10
Citric acid (CA)	1 – 300	$6\times10^{-2} - 60$

a) Concentrations in ice refer to the pre-frozen concentrations in the liquid solutions.

Chromophoric dissolved organic matter (CDOM), of which humic acid (HA) is a major component, is present at concentrations up to a few 10's of mg/L of carbon in surface waters.[44, 45] Concentrations in polar snow and ice are somewhat lower (often less than 1 mg/L), but concentrations greater than 10 mg/L have been reported.[37-39, 46, 47] The humic acid concentrations used in this study span this range. Detergent surfactants, from household or industrial use, are often present in surface waters, and concentrations of 100's of mg/L have been reported in laundry wastewater.[48] Sodium dodecyl sulphate (SDS) is used as a reference surfactant in this work. Due to sensitivity constraints, the concentrations used were higher than reported environmental levels. Two concentrations were chosen: one above and one below the critical micelle concentration (~2.3 g/L).[49] Citric acid was used to represent smaller oxidized OM at concentrations spanning 3 orders of magnitude.

Samples were frozen in a previously-described[23] custom-built cold chamber with a stainless steel baseplate and an air-tight cover containing a 1 mm thick quartz window. A ~100 µL drop of liquid sample was placed on the baseplate and the temperature was controlled with a single-stage Peltier cooler. A thermocouple junction, inserted in the sample prior to freezing, was used to monitor the temperature of the sample in real time. Unless otherwise stated, the temperature of the sample was slowly decreased until it visibly froze, and then the temperature was varied between –5 °C to –25 °C in –5 °C steps. After allowing about 10 minutes to equilibrate at each temperature, Raman maps were acquired by scanning over an area in the horizontal plane (surface maps) or vertical plane (depth maps) for each sample. The temperature was kept constant within ±0.5 °C during the scanning process.

Raman measurements

Raman scattering emission was measured using a Renishaw Invia Basis Raman microscope with a green laser (wavelength 532 nm). The sample stage was placed on the three-axis translation stage of the microscope. A dry objective of 0.5 numerical aperture, 50× magnification, and 8.2 mm working distance was used to focus the excitation light on the sample through the quartz window of the stage. Scattering response of the samples was acquired using a 1015-pixel charge coupled device (CCD) following diffraction from the grating. In all experiments, the range of Raman shifts acquired was between 2502 cm^{-1} and 3826 cm^{-1}, which allowed us to acquire the Raman spectrum of the O–H stretch region of DI water and/or ice simultaneously with the C–H stretch bands from SDS or citric acid, as well as broad featureless fluorescence emission from humic acid.

All spectral data were analysed in Matlab (R2011a). The data analysis procedure followed this sequence for each acquired spectrum: (i) non-linear (3^{rd} order polynomial) background estimation; (ii) background subtraction to extract the Raman scattering spectrum; (iii) evaluation of solute-specific intensity of emission relative to the global peak in the emission band; (iv) decomposition of the O–H stretching region in the spectrum into fractional spectral contributions from pure ice and unfrozen solution. Depending on the solute type, either the C–H stretch peak (for SDS and citric acid) or the mean fluorescence background (for humic acid) was used in step (iii). A full description of step (iv) is provided in the *Supplementary Material*.

Raman surface maps were acquired by scanning a 150 μm × 150 μm area of the surface with 3 μm steps. The surface plane was identified visually using the optical microscope attachment of the instrument. Depth maps were acquired over a vertical plane of 200 μm height and 150 μm width with 10 μm steps in the vertical direction and 3 μm steps in the horizontal direction. For all acquired maps, integration time was 1 sec. Surface maps took approximately 56 minutes and depth maps took approximately 20 minutes. For each solute type and concentration, Raman maps were acquired over the same area at different temperatures. Each experiment was repeated on at least 3 separate samples for each condition. At each coordinate, the spectral data was analysed using the four steps described in the previous paragraph.

Results and Discussion

Spectra

FIG 1(a) shows typical spectra of solid humic acid, SDS, and citric acid, and FIG. 1(b) shows spectra of pure DI water and of aqueous solutions containing humic acid, SDS, or citric acid at room temperature. The broad peak centred around 3415 cm^{-1} in each aqueous sample is due to stretching of O–H bonds in hydrogen-bonded water. The shape of this peak is generally attributed to, and can be deconvoluted among, between three and eight[50-52] different Gaussian peaks originating from different combinations of hydrogen

bond donor and acceptor water molecules. The humic acid spectrum is characterized by a large fluorescence background both as a solid sample and dissolved in aqueous solution, while SDS and citric acid show Raman peaks corresponding to their C–H stretching bands between 2800 cm^{-1} and 3100 cm^{-1} with relatively small fluorescence backgrounds. FIG. 1(c) shows spectra acquired from the surface of frozen aqueous solutions of humic acid, SDS, and citric acid, as well as of frozen DI water at −15 °C. Raman C–H stretch peaks of SDS and citric acid, as well as fluorescence from humic acid and, to a smaller extent, from SDS and citric acid, were clearly seen at the air-ice interface. The shape of the O–H stretching region of ice is different from that in the liquid phase, with maximum intensity observed at ~3135 cm^{-1} indicating a more extensive hydrogen bonding network.[53] An increase in intensity in the high-energy shoulder of the O–H stretch band of ice (~3415 cm^{-1}) relative to the peak (~3135 cm^{-1}) that is not fully explained by background fluorescence was observed in the presence of each solute. We attribute this spectral shift to the presence of liquid water, as we have described previously.[23] As discussed in detail in the following section, it likely arises from solute-induced surface melting. It is possible that the O–H stretches of citric acid (at 3290 cm^{-1} and 3495 cm^{-1} in liquid aqueous solution) have some effect on the shape of the observed O–H stretch; we cannot currently quantify this. However, surface melting (rather than artefacts from C–H stretches) is likely the major cause of the shifts in the O–H band; similar shifts are observed in the presence of SDS, which does not contain hydroxyl functional groups, and humic acid, for which only fluorescence emission is detected in this spectral region using 532 nm excitation.

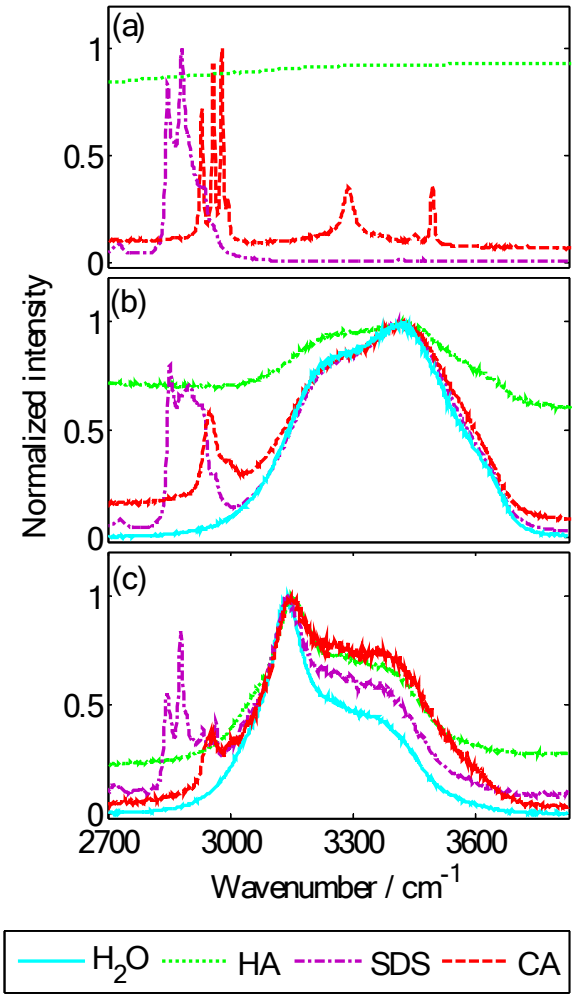

FIG. 1: Emission spectra of (a) solid HA, SDS, and CA at 25 °C; (b) DI water and of aqueous solutions of HA (30 mg/L), SDS (200 g/L), and CA (300 g/L) at 25 °C; and (c) DI water ice and frozen aqueous solutions containing HA (3 mg/L), SDS (1 g/L), and CA (6 g/L) at −15 °C.

Emission intensities of each solute relative to emission from the O–H stretch band of water were much greater in the frozen samples than in the liquid. Although similar intensities of the C–H stretch peaks of SDS and citric acid were observed in panels (b) and (c), the initial (pre-frozen) concentrations of SDS and citric acid required to generate this signal in ice were 0.5% and 2% of those in the liquid phase. Limits of detection (LOD) in the liquid phase were 1 mg/L (HA), 10 g/L (SDS), and 20 g/L (CA) (see the *Supplementary Material* for further discussion). The humic acid detection limit was much lower than that of SDS or citric acid because fluorescence is a much stronger process than Raman scattering. We did not establish LOD for frozen samples, but strong emission from all three solutes was observed at concentrations one to two orders of magnitude lower than the corresponding LOD in liquid water (0.3 mg/L HA, 1 g/L

SDS, and 0.06 g/L CA). This is likely due to local concentration enhancements at the surface caused by freeze-exclusion.

We can use the spectra in FIG. 1 to make inferences about the solvation state of the solutes. The C–H Raman stretch of SDS in liquid water was less resolved than that in the dry sample, and the relative intensities of the asymmetric and symmetric C–H stretches at 2882 cm^{-1} and 2848 cm^{-1} respectively were reversed in the liquid and solid samples. Both of these changes reflect the fact that SDS is solvated in aqueous solution.[54, 55] The SDS C–H stretch band at the ice surface resembled that of solid SDS: the asymmetric and symmetric stretches were clearly resolved, and the relative intensities matched those in the solid sample. This suggests that SDS is not appreciably solvated at the air-ice interface. Conversely, peak broadening of the C–H stretch bands of citric acid was observed in ice samples as well as in aqueous solution, suggesting that, unlike SDS, citric acid is solvated at the air-ice interface. Raman emission was not observed for humic acid in any samples.

Surface Maps

Surface maps were acquired at air-ice interfaces between −5 °C and −25 °C. FIG. 2 shows representative surface maps for frozen aqueous solutions of humic acid, SDS, and citric acid at −15 °C. Corresponding maps at −5 °C and −25 °C are shown in FIG. S6 – S8 in the *Supplementary Material*. The left column in the maps shows normalized intensities of humic acid fluorescence and of SDS and citric acid Raman scattering as a function of location. Variations in normalized intensity suggest that concentration (or film depth) may vary spatially, but we cannot currently quantify solute concentrations at ice surfaces. This is due to two main factors. First, SDS and possibly humic acid appear not to be dissolved within liquid regions in frozen solution. The calibration curves presented in Figure S4 of the *Supplementary Material* can only relate normalized intensity to concentration for solvated species. Second, each spectrum reflects the average signal over some volume that is determined by laser spot size and depth resolution. This volume will often contain a heterogeneous distribution of solute concentrations, including regions with no solute. The defined features in the normalized intensity maps of SDS and humic acid may be indicative of 3-dimensional structures at the air-ice interface, consistent with the presence of non-solvated organic films. The normalized intensity of citric acid is much more spatially uniform, as would be expected for a molecule dissolved in aqueous solution.

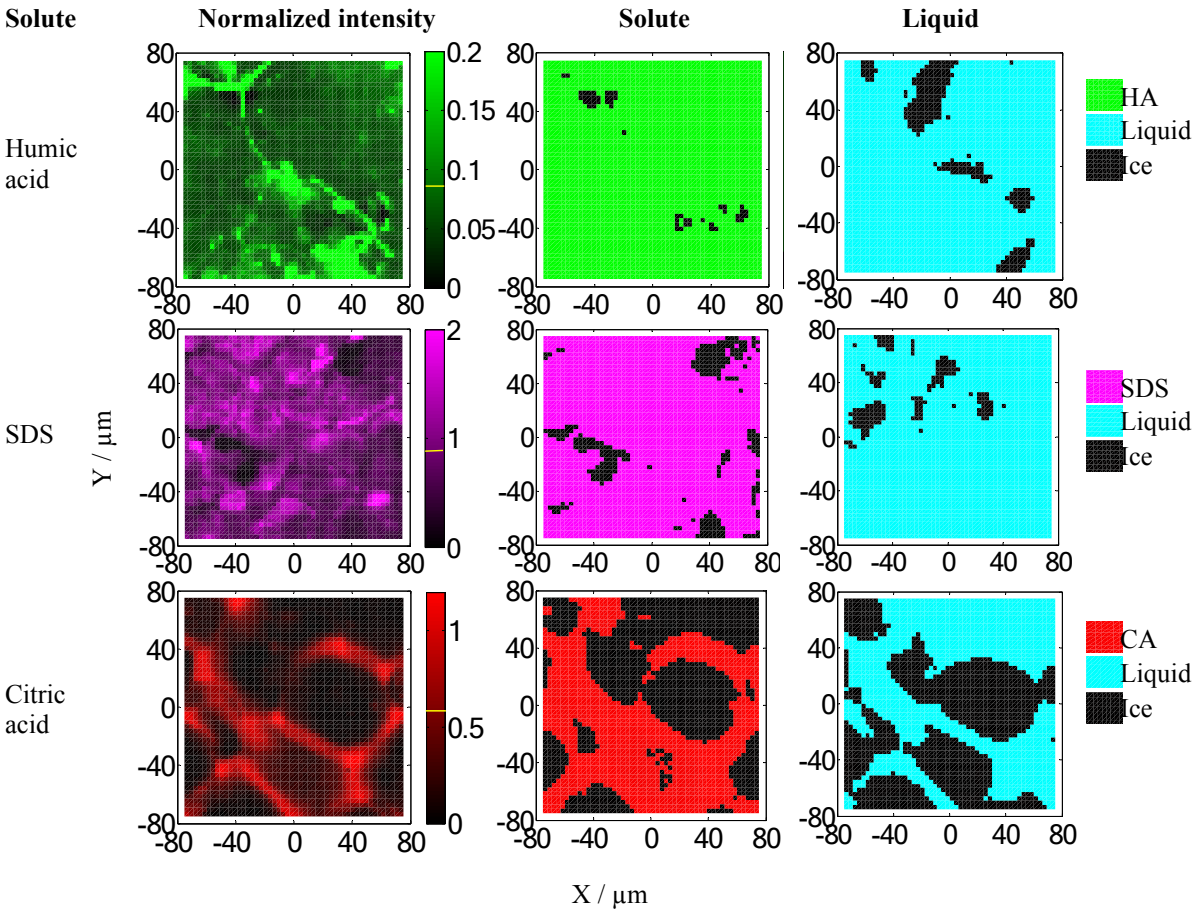

FIG. 2: Surface maps of emission intensities normalized to 3135 cm^{-1} (left column), solute surface coverage (middle column), and surface coverage of liquid water (right column) for humic acid, SDS, and citric acid solutions with bulk (pre-frozen) concentrations of 3 mg/L (HA), 1 g/L (SDS) and 60 g/L (CA). *X* and *Y* represent two orthogonal directions on the surface. All measurements were acquired at −15 °C. The scan area is 150 μm × 150 μm with a step size of 3 μm. The mean normalized emission intensity from each solute is shown as a yellow horizontal line in the corresponding colour-bar in the left column.

The middle column of FIG. 2 shows the distribution of organic solutes across the ice surface (as determined by a method discussed in the *Supplementary Material*). After background subtraction, the O–H stretching region in the spectrum at each coordinate was quantitatively deconstructed into contributions from pure ice and liquid water in a method described in the *Supplementary Material*. A threshold value for spectral liquid contribution (x_W, described in the *Supplementary Material*) was used to classify each spectrum as either ice or liquid water. The distribution of liquid water at the air-ice interface is shown in the right-hand column. Citric acid surface coverage was much less extensive than that of humic acid or SDS, even at very high citric acid concentrations (60 g/L). The extent of fractional liquid surface coverage (θ_w, calculated as the fraction of pixels in the maps in the right column that were determined to correspond to liquid water) was also quite different for samples containing citric acid compared to those containing

humic acid or SDS. In contrast to the near-complete liquid coverage observed in samples containing humic acid or SDS, citric acid samples contained channel-like liquid structures.

While solute and liquid fractional surface coverage were both very high for samples containing humic acid or SDS, the locations of liquid water and of organic solute may not be strongly correlated. Specifically, FIG. 2 shows that some regions that did not contain organic solute contained liquid water, and that some regions that did not contain liquid water contained organic solute. We analysed the spatial correlation between solutes and liquid water from the maps of normalized intensities and x_W to better quantify the spatial correlation (or lack thereof) between organic solutes and liquid water at ice surfaces. FIG. 3 shows Pearson correlation coefficients, ρ_{SW}, at different temperatures for all frozen samples (for humic acid, normalized intensity maps could not be measured at concentrations below 0.3 mg/L, so data from these samples are not shown). Despite near-complete surface coverage by liquid water and solute for a wide range of solute concentrations and temperatures, humic acid and SDS were not spatially correlated with liquid water at ice surfaces with an average ρ_{sw} of 0.05 ± 0.13. Conversely, there was a strong positive correlation (ρ_{SW} = 0.63 ± 0.07) between citric acid and liquid water irrespective of temperature and concentration, which suggests that citric acid is generally co-located with liquid water, likely in liquid channels as suggested by FIG. 2 and as has been reported for a number of ionic solutes.[17, 22-25, 27, 28, 56]

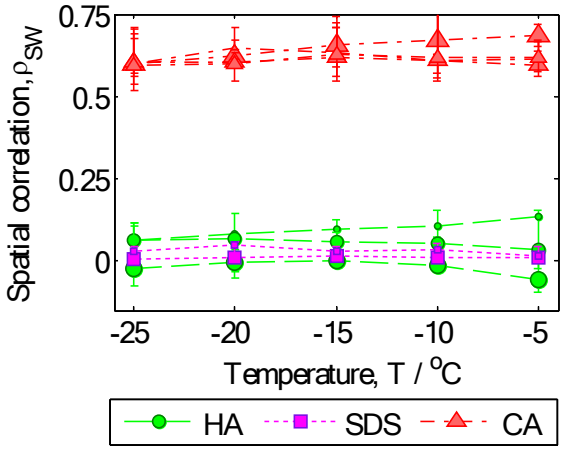

FIG. 3: Spatial correlation of solute emission intensity and spectral liquid contribution, x_W, at the air-ice interface of frozen solutions of HA (0.3 mg/L, 3 mg/L, and 30 mg/L), SDS (1 g/L and 10 g/L), and CA (0.06 g/L, 0.6 g/L, 6 g/L, and 60 g/L). Increasing marker size represents increasing pre-frozen solution concentrations.

FIG. 4 shows the fractional surface coverage, θ_W, at air-ice interfaces as a function of pre-frozen solute concentration at different temperatures. Positive concentration dependences were observed for all three solutes, except at high HA and SDS concentrations and high temperatures when θ_W was close to 100%. Samples containing citric acid had lower surface coverage than SDS and humic acid at all

temperatures, despite pre-frozen citric acid concentrations that were similar to SDS and up to five orders of magnitude higher than humic acid. This suggests that all three organic solutes induce surface melting, but that humic acid and SDS do so more effectively (i.e., at much lower concentrations) than citric acid. The effect of temperature on the fractional surface coverage can also be observed from this figure by tracking markers from small (low temperature) to large (high temperature) at a fixed solute concentration. A positive temperature dependence was observed for all solutes at all concentrations, with the exception of SDS at 10 g/L; at this concentration the ice surface was completely covered with liquid water at all temperatures. The magnitude of the temperature dependence decreased for humic acid and SDS as concentrations increased, likely because the surface became saturated with liquid water at increasingly low temperatures. For samples containing citric acid, the temperature dependence became larger with increasing solute concentration. This is similar to the dependence we observed in frozen aqueous NaCl solutions,[23] and is qualitatively consistent with the thermodynamically-predicted temperature dependence of a frozen binary solution.[21, 23] The temperature dependence of fractional surface coverage is explicitly plotted in FIG. S9 in the *Supplementary Material*.

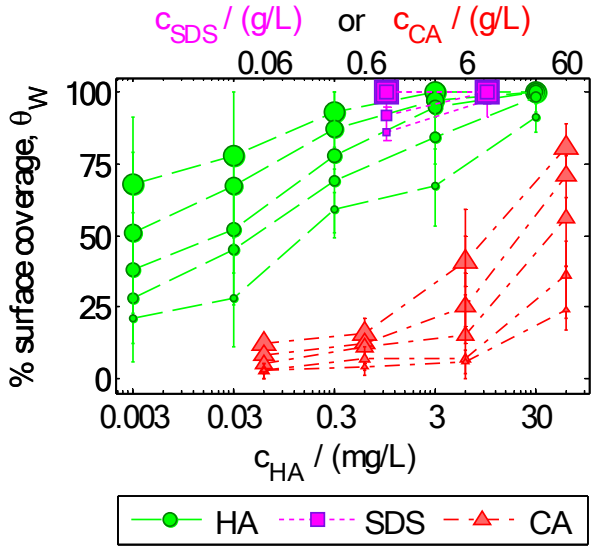

FIG. 4: Effect of pre-frozen solute concentration on fractional liquid surface coverage. The horizontal axes are in mg/L for HA (ticks at the bottom) and in g/L for SDS and CA (ticks at the top) in log scale. Increasing marker size indicates increasing temperature from –25 °C to –5 °C in 5 °C steps. Error bars represent the standard deviation of measurements from three samples. Dashed traces are included to guide the eye.

As discussed above, the amount of liquid present at the air-ice interface generally increased with increasing temperature. If solutes are dissolved in liquid regions, we would expect an inverse relationship

between observed solute concentrations (which likely correlate with normalized emission intensity) and temperature due to solute dilution with increasing liquid fraction. FIG. 5 shows averaged normalized emission intensity of the frozen solutions as a function of temperature. These values were determined from surface maps of emission spectra of each frozen solution by calculating the average intensity in the solute-covered regions. Citric acid Raman intensity decreased with increasing temperature, as expected for a solute that is dissolved in liquid water. Conversely, emission intensities of humic acid and SDS were largely insensitive to temperature. Some variation was observed for the highest humic acid concentration (30 mg/L), but these data have very high sample-to-sample variation as reflected by the large error bars. These observations support our conclusion that citric acid is solvated in liquid water at the air-ice interface, but that humic acid and SDS are not largely solvated.

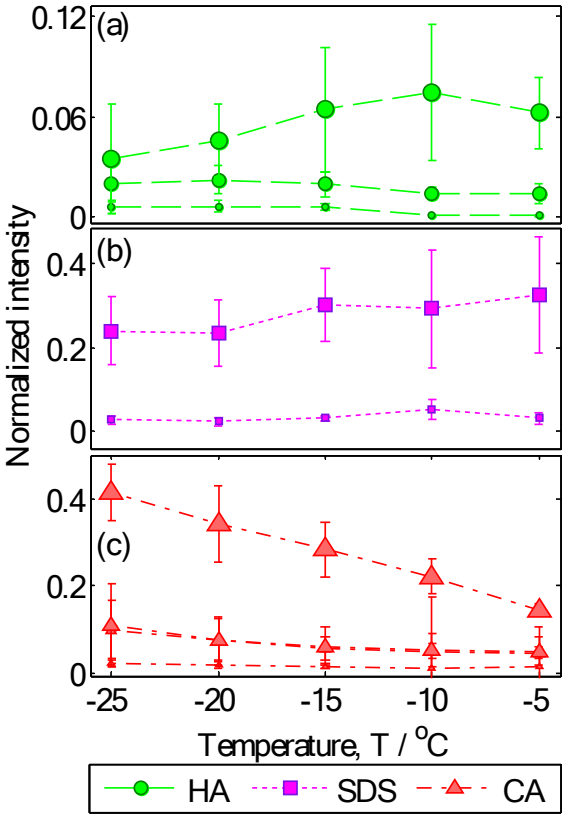

FIG. 5: (a) Fluorescence intensity of HA; (b) Raman intensity of SDS; and (c) Raman intensity of CA as a function of temperature at the air-ice interface. Increasing marker size indicates an increase of pre-frozen concentration. c_{HA} = 0.3 mg/L, 3 mg/L and 30 mg/L, c_{SDS} = 1 g/L and 10 g/L, and c_{CA}= 0.06 g/L, 0.6 g/L, 6 g/L, and 60 g/L. Error bars represent the standard deviation of measurements from three samples.

Depth Profiles

FIG. 6(a) through (c) show depth slices of normalized intensity for the frozen humic acid, SDS, and citric acid samples for which surface maps are shown in FIG. 2 at −15 °C. The observed intensity above the ice surface is an artefact due to contributions from solutes at the ice surface when the incident laser beam was focused above the sample. Depth resolution within the ice was approximately 20 μm. We note that citric acid and SDS solutions have negligible molar absorptivity at 532 nm while humic acid absorbs much more strongly at that wavelength. However, since the intensities are normalized to the peak intensity within the same acquired spectrum at each spot, the effect of a gradual decrease in actual count-rates due to absorption, if any, is negated. Similarly, any effect of the dead-time of the detector on the mapped intensities in the surface and depth profiles, although highly unlikely in the default optimum operating mode of the detector, is also negated by the normalization. The apparent gradual decrease in solute intensity with depth is, rather, due to the poor depth resolution; the true thickness of the film is likely much smaller than the apparent thickness from the maps. We therefore used these depth profiles only to qualitatively analyze the distribution of solutes throughout the ice sample, rather than to quantify organic layer thicknesses.

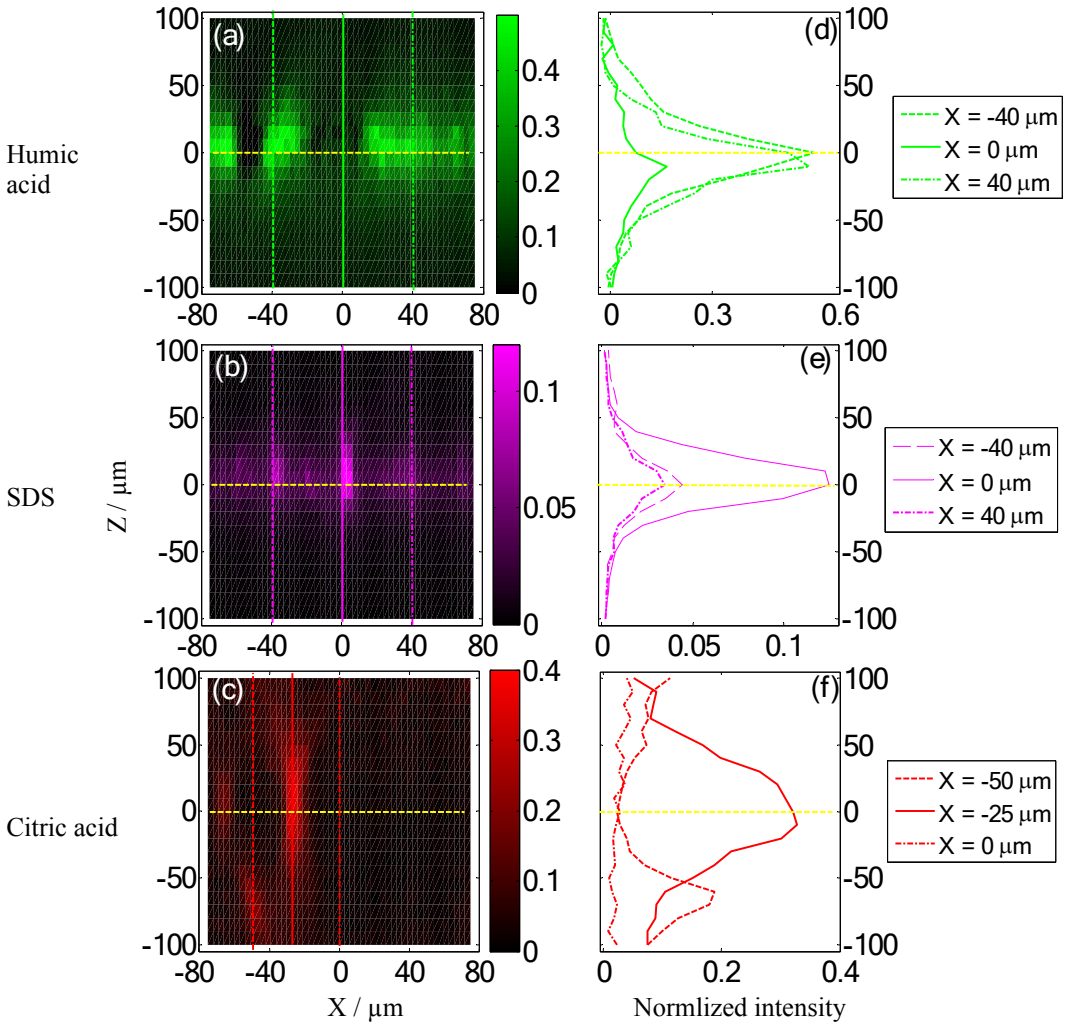

FIG. 6: Depth slices in the *X*-*Z* plane of normalized intensities at −15 °C for frozen aqueous solutions containing (a) HA (3 mg/L), (b) SDS (1 g/L), and (c) CA (60 g/L). Concentrations refer to those in the pre-frozen solutions. *Z* is the vertical axis extending from above the sample (positive values) to inside the sample (negative values). *Z* = 0 is referenced at the surface and shown by the yellow horizontal lines. Slices were scanned over a length of 150 μm laterally with a 3 μm step size and 200 μm vertically with a 10 μm step size. Depth profiles at three values of *X* (shown on the maps) are shown in (d), (e), and (f) for HA, SDS, and CA respectively.

The plots of intensities along the vertical lines in the maps are displayed in FIG. 6(d) and (e) for humic acid and SDS respectively, showing the continuous Lorenzian decrease in intensity from the surface. It is noteworthy that in no situations did we observe signal corresponding to humic acid or SDS deep inside the sample, indicating that these solutes reside predominantly at the surface due to freeze exclusion. This suggests that the concentration of the solutes at the air-ice interface would be significantly higher than their initial bulk concentrations in the liquid phase, although, as described above, the concentrations cannot be quantified at present. Depth slices of Raman intensity of a frozen citric acid solution in FIG. 6(f) shows solute distributed heterogeneously throughout the sample, including at much greater depths than those at

which humic acid or SDS were detected. The plot in FIG. 6(f) at $X = -50$ μm shows the presence of citric acid at an apparent depth of 60 μm (equivalent to true depth of ~80 μm due to the refractive index of ice). This citric acid does not appear to be connected to the ice surface, which suggests that citric acid is not completely excluded to the surface, but is distributed between liquid regions within the bulk and at the air-ice interface. This is similar to observations we recently made about NaCl brine in frozen solutions,[23] and is consistent with studies on Cl^- and NO_3^- ions in frozen aqueous solutions that reported surface concentrations lower than those expected if all the solute was excluded to the surface. [57-60]

Atmospheric Implications

Our results suggest different behaviour of humic acid and SDS compared to citric acid in frozen aqueous solutions. We suggest that humic acid and SDS are almost fully excluded to the air-ice interface where they form films that coat most of the surface at most temperatures and pre-frozen solute concentrations. A layer of liquid water at the ice surface is observed in their presence. Humic acid and SDS appear not to be appreciably solvated by this liquid water layer. These results are consistent with organic films residing above (rather than within) the liquid water layer. Unlike humic acid and SDS, citric acid is excluded to liquid regions throughout the ice sample, including (but not limited to) the air-ice interface. It appears to be solvated within liquid channels and pockets in the sample, and it causes some surface melting, but to a much lesser extent than humic acid and SDS. The distribution of citric acid in ice is similar to reported distributions of ionic species,[22-25, 31] including distributions of Cl^- that we recently inferred using Raman microscopy.[23]

The effects of OM on the physical and chemical properties of air-ice interfaces are important to our understanding of, and ability to predict, reaction rates in snow-covered regions. Reactivity at air-ice interfaces has been reported to differ greatly from that in bulk liquid aqueous solution or at air-liquid water interfaces.[2, 3, 5] As discussed in the Introduction, a few studies have investigated the effects of dissolved organic matter on reaction kinetics in ice and at air-ice interfaces. Dissolved organic matter including fulvic acid and humic acid were reported to increase photolysis rates of the insecticide aldrin in ice samples due to indirect photolysis such as photosensitization and singlet oxygen formation.[37] Photolysis in frozen samples ranged from ~3 to > 20 times faster than in liquid samples, depending on the type of CDOM present. These enhancements were attributed to freeze concentration effects, consistent with our interpretation of the Raman maps of humic acid in this work.

We recently investigated the effects of organic molecules (octanol, decanol, and fulvic acid) on the photolysis kinetics of polycyclic aromatic hydrocarbons (PAHs).[9, 10] All three types of OM suppressed PAH photolysis, but the mechanisms were different. We attributed suppression by octanol and decanol, which

do not absorb sunlight, to decreased local polarity,[9] while suppression by fulvic acid was primarily due to competitive photon absorption (the "inner filter effect").[10] Our current results are consistent with both of these mechanisms, and are also consistent with suppression being due to increased liquid water fractions in the presence of surface-active OM, since many aromatic pollutants, including PAHs, have been reported to photolyze more rapidly at air-ice interfaces than at air-liquid water interfaces or in bulk liquid water.[3, 4]

To our knowledge, the effects of small, polar organic molecules on chemistry in ice have not been investigated. We suggest that organic species similar to citric acid will affect reactivity in ice primarily via solute-induced melting. Based on the fractional liquid surface coverages we report in FIG. 4(a), we predict that surface melting will be small, with fractional liquid coverages generally lower than 10% at environmentally-relevant OM concentrations. This small amount of liquid water could measurably affect reaction kinetics, however. For example, we showed that photolysis of the aromatic compound harmine, which is ~4 times faster at air-ice interfaces than at air-liquid water interfaces, was suppressed by NaCl and NaBr at ice surfaces due to solute-induced surface melting.[11] Based on that work and our recent investigation of the effects of NaCl on fractional liquid surface coverages at air-ice interfaces,[23] we predict that when 10% of the ice surface is coated with liquid water, harmine's photolysis rate would be reduced by a similar amount (~10%). It is therefore possible that environmentally-relevant concentrations of small organic molecules could affect reaction kinetics via solute-induced melting, even without considering other potential effects such as altered local polarity, indirect photolysis, or altered air-ice partitioning.

We conclude by noting that solutes generally do not exist in isolation. Most aqueous atmospheric systems (whether liquid or frozen) contain multiple solutes. The effects of co-solutes on solute distribution and liquid volume fractions in frozen aqueous solutions have not been widely reported, and it is possible that effects are not additive. Future studies combining Raman microscopy or other surface-sensitive techniques with complementary techniques such as x-ray micro-computed tomography would provide a complete picture of solute distributions throughout entire ice samples, and would greatly further our understanding of physical and chemical processes in – and at the surface of – snow and ice in the environment.

Acknowledgements

This work was funded by National Science Foundation (NSF) Award 1454959.

References

1 Domine F, Shepson PB. Air-snow interactions and atmospheric chemistry. *Science*. 2002 Aug; 297: 1506−1510.

2 Grannas AM, Jones AE, Dibb J, Ammann M, Anastasio C, Beine HJ, et al. An overview of snow photochemistry: evidence, mechanisms and impacts. *Atmospheric Chemistry and Physics*. 2007 Aug; 7: 4329−4373.

3 Kahan TF, Philip Malley PPA, Grossman JN, Stathis AA. Photochemistry in model aqueous-organic atmospheric condensed phases. *ACS Symposium Series, Chapter 5*. American Chemical Society: Washington, DC. 2018 Jan; 87–103.

4 Kahan TF, Wren SN and Donaldson DJ. A pinch of salt is all it takes: Chemistry at the frozen water surface. *Accounts of Chemical Research*. 2014 May; 47: 1587−1594.

5 Bartels-Rausch T, Jacobi HW, Kahan TF, Thomas JL, Thomson ES, Abbatt JPD, et al. A review of air-ice chemical and physical interactions (AICI): liquids, quasi-liquids and solids in snow. *Atmospheric Chemistry and Physics*. 2014 Feb; 14: 1587–1633.

6 Kahan TF, Zhao R, Donaldson DJ. Hydroxyl radical reactivity at the air-ice interface. *Atmospheric Chemistry and Physics*. 2010 Jan; 10: 843− 854.

7 Stathis AA, Hendrickson-Stives AK, Kahan TF. Photolysis kinetics of toluene, ethylbenzene, and xylenes at ice surfaces. *Journal of Physical Chemistry A*. 2016 Aug; 120: 6693−6697.

8 Kahan TF, Donaldson DJ. Photolysis of polycyclic aromatic hydrocarbons on water and ice surfaces. *Journal of Physical Chemistry A*. 2007 Jan; 111: 1277–1285.

9 Malley PPA, Kahan TF. Nonchromophoric organic matter suppresses polycyclic aromatic hydrocarbon photolysis in ice and at ice surfaces. *Journal of Physical Chemistry A*. 2014 Feb; 118: 1638−1643.

10 Malley PPA, Grossman JN, Kahan TF. Effects of chromophoric dissolved organic matter on anthracene photolysis kinetics in aqueous solution and ice. *Journal of Physical Chemistry A*. 2017 Sept; 121: 7619−7626.

11 Kahan TF, Kwamena NOA, Donaldson DJ. Different photolysis kinetics at the surface of frozen freshwater vs. frozen salt solutions. *Atmospheric Chemistry and Physics*. 2010 Nov; 10: 10917−10922.

12 Kahan TF, Donaldson DJ. Benzene photolysis on ice: Implications for the fate of organic contaminants in the winter. *Environmental Science and Technology*. 2010 Apr; 44: 3819−3824.

13 Ray D, Kurkova R, Hovorkova I, Klan P. Determination of the specific surface area of snow using ozonation of 1,1-diphenylethylene. *Environmental Science and Technology*. 2011 Nov; 45: 10061−10067.

14 Ray D, Liskova H, Klan P. Kinetics of heterogeneous reactions of ozone with representative PAHs and an alkene at the air–ice interface at 258 and 188 K. *Environmental Science-Processes & Impacts*. 2014 Apr; 16: 770−776.

15 Ray D, Malongwe JK, Klan P. Rate acceleration of the heterogeneous reaction of ozone with a model alkene at the air–ice interface at low temperatures. *Environmental Science and Technology*. 2013 Jul; 47: 6773−6780.

16 Kahan TF, Donaldson DJ. Heterogeneous ozonation kinetics of phenanthrene at the air–ice interface. *Environmental Research Letters.* 2008 Nov; 3; 045006.

17 Hullar T, Anastasio C. Yields of hydrogen peroxide from the reaction of hydroxyl radical with organic compounds in solution and ice. *Atmospheric Chemistry and Physics*. 2011 Jul; 11: 7209–7222.

18 Hudait A, Allen MT, Molinero V. Sink or swim: ions and organics at the ice–air interface. *Journal of the American Chemical Society.* 2017 Jun; 139: 10095−10103.

19 Vrbka L, Jungwirth P. Brine rejection from freezing salt solutions: A molecular dynamics study. *Physical Review Letters*. 2005 Sept; 95: 148501.

20 Bauerecker S, Ulbig P, Buch V, Vrbka L, Jungwirth P. Monitoring ice nucleation in pure and salty water via high-speed imaging and computer simulations. *Journal of Physical Chemistry C*. 2008 May; 112: 7631–7636.

21 Cho H, Shepson PB, Barrie LA, Cowin JP, Zaveri R. NMR investigation of the quasi-brine layer in ice/brine mixtures. *Journal of Physical Chemistry B*. 2002 Oct; 106: 11226–11232.

22 McCarthy C, Blackford JR, Jeffree CE. Low-temperature-SEM study of dihedral angles in the ice-I/sulfuric acid partially molten system. *Journal of Microscopy*. 2012 Dec; 249: 150–157.

23 Malley PPA, Chakraborty S, Kahan TF. Physical characterization of frozen saltwater solutions using Raman microscopy. *ACS Earth and Space Chemistry*. 2018 May; 2(7): 702–710.

24 Krausko J, Runstuk J, Nedela V, Klan P, Heger D. Observation of a brine layer on an ice surface with an environmental scanning electron microscope at higher pressures and temperatures. *Langmuir*. 2014 Apr; 30(19): 5441−5447.

25 Liyana-Arachchi TP, Valsaraj KT, Hung FR. Adsorption of naphthalene and ozone on atmospheric air/ice interfaces coated with surfactants: A molecular simulation study. *Journal of Physical Chemistry A*. 2012 Mar; 116: 2519–2528.

26 McNeill VF, Grannas AM, Abbatt JPD, Ammann M, Ariya P, Bartels-Rausch T, et al. Organics in environmental ices: sources, chemistry, and impacts. *Atmospheric Chemistry and Physics*. 2012 Oct; 12: 9653–9678.

27 McNeill VF, Geiger FM, Loerting T, Trout BL, Molina LT, Molina MJ. Interaction of hydrogen chloride with ice surfaces: The effects of grain size, surface roughness, and surface disorder. *Journal of Physical Chemistry B*. 2007 Jun; 111: 6274–6284.

28 Blackford JR, Jeffree CE, Noake DFJ, Marmo BA. Microstructural evolution in sintered ice particles containing NaCl observed by low-temperature scanning electron microscope. *Proceedings of the Institution of Mechanical Engineers, Part L: Journal of Materials: Design and Applications.* 2007 Jul; 221: 151−156.

29 Yang X, Nedela V, Runstuk J, Ondruskova G, Krausko J, Vetrakova L, Heger D. Evaporating brine from frost flowers with electron microscopy and implications for atmospheric chemistry and sea-salt aerosol formation. *Atmospheric Chemistry and Physics*. 2017 May; 17: 6291−6303.

30 Bluhm H, Ogletree DF, Fadley CS, Hussain Z, Salmeron M. The premelting of ice studied with photoelectron spectroscopy. *Journal of Physics: Condensed Matter*. 2002 Feb; 14: L227–L233.

31 Tokumasu K, Harada M, Okada T. X-ray fluorescence imaging of frozen aqueous NaCl solutions. *Langmuir*. 2016 Dec: 32(2): 527–533.

32 Mmereki BT, Chaudhuri SR, Donaldson DJ. Enhanced uptake of PAHs by organic-coated aqueous surfaces. *Journal of Physical Chemistry A*. 2003 Mar; 107: 2264–2269.

33 Donaldson DJ, Mmereki BT, Chaudhuri SR, Handley S, Oh M. Uptake and reaction of atmospheric organic vapours on organic films. *Faraday Discussions*. 2005 Apr; 130: 227–239.

34 Donaldson DJ, Vaida V. The influence of organic films at the air−aqueous boundary on atmospheric processes. *Chemical Reviews*. 2006 Apr; 106(4): 1445–1461.

35 Ryder OS, Campbell NR, Morris H, Forestieri S, Ruppel MJ, Cappa C, et al. Role of organic coatings in regulating N_2O_5 reactive uptake to sea spray aerosol. *Journal of Physical Chemistry A*. 2015 Nov; 119, 11683–11692.

36 Nathanson GM, Davidovits P, Worsnop DR, Kolb CE. Dynamics and kinetics at the gas-liquid interface. *Journal of Physical Chemistry*. 1996 Aug; 100: 13007-13020.

37 Grannas AM, Pagano LP, Pierce BC, Bobby R, Fede A. Role of dissolved organic matter in ice photochemistry. *Environmental Science and Technology*. 2014 Aug; 48: 10725–10733.

38 Fede A, Grannas AM. Photochemical production of singlet oxygen from dissolved organic matter in ice. *Environmental Science and Technol*ogy. 2015 Oct; 49(21): 12808–12815).

39 Grannas AM, Shepson PB, Filley TR. Photochemistry and nature of organic matter in arctic and antarctic snow. *Global Biogeochemical Cycles.* 2004 Jan; 18(1), Gb1006.

40 Bartels-Rausch T, Brigante M, Elshorbany YF, Ammanna M, D'Anna B, George C, et al. Humic acid in ice: Photo-enhanced conversion of nitrogen dioxide into nitrous acid. *Atmospheric Environment*. 2010 Dec; 44: 5443−5450.

41 Heger D, Klan P. Interactions of organic molecules at grain boundaries in ice: A solvatochromic analysis. *Journal of Photochemistry and Photobiology A: Chemistry*. 2007 Apr; 187: 275–284.

42 Heger D, Klanova J, P. Klan. Enhanced protonation of cresol red in acidic aqueous solutions caused by freezing. *Journal of Physical Chemistry B*. 2006 Jan; 110: 1277–1287.

43 Cheng J, Soetjipto C, Hoffmann MR, Colussi AJ. Confocal fluorescence microscopy of the morphology and composition of interstitial fluids in freezing electrolyte solutions. *Journal of Physical Chemistry Letters*. 2010 Jan; 1: 374–378.

44 Serkiz SM, Perdue EM. Isolation of dissolved organic matter from the Suwannee river using reverse osmosis. *Water Research*. 1990 Jul; 24(7): 911–916.

45 Mantoura RFC, Woodward EMS. Conservative behaviour of riverine dissolved organic carbon in the Severn Estuary: chemical and geochemical implications. *Geochimica et Cosmochimica Acta*. 1983 Jul; 47(7), 1293–1309.

46 Grannas AM, Cory RM, Miller PL, Chin YP, McKnight DM. The role of dissolved organic matter in arctic surface waters in the photolysis of hexachlorobenzene and lindane. *Journal of Geophysical Research-Biogeosciences.* 2012 Jan; 117, G01003.

47 Fellman JB, Hood E, Raymond PA, Stubbins A, Spencer RGM. Spatial variation in the origin of dissolved organic carbon in snow on the Juneau icefield, Southeast Alaska. *Environmental Science and Technology*, 2015 Sept; 49(19): 11492–11499.

48 Ramcharan T, Bissessur A. Analysis of linear alkylbenzene sulfonate in laundry wastewater by HPLC–UV and UV–Vis spectrophotometry. *Journal of Surfactants and Detergents*. 2016 Jan; 19: 209–218.

49 Fuguet E, Rafols C, Roses M, Bosch E. Critical micelle concentration of surfactants in aqueous buffered and unbuffered systems. *Analytica Chimica Acta*. 2005 Aug; 548: 95–100.

50 Choe C, Lademanna J, Darvin ME. Depth profiles of hydrogen bound water molecule types and their relation to lipid and protein interaction in the human stratum corneum in vivo. *Analyst*. 2016 Oct; 141: 6329–6337.

51 Schmidt DA, Miki K. Defective continuous hydrogen-bond networks: An alternative interpretation of IR spectroscopy. *ChemPhysChem.* 2008 Sept; 9: 1914–1919.

52 Max JJ, Chapados C. Isotope effects in liquid water by infrared spectroscopy. *Journal of Chemical Physics*. 2002 Mar; 116: 4626–4642.

53 Sun Q, Zheng H. Raman OH stretching vibration of ice I_h. *Progress in Natural Science*. 2009 Nov;19: 1651–1654.

54 M. Picquart. Vibrational model behavior of SDS aqueous solutions studied by Raman scattering. *Journal of Physical Chemistry.* 1986 Jan; 90: 243–250.

55 Cazzolli G, Caponi S, Defant A, Gambi CMC, Marchetti S, Mattarelli M, et al. Aggregation processes in micellar solutions: a Raman study. *Journal of Raman Spectroscoscopy*. 2012 Dec; 43: 1877–1883.

56 Lieb-Lappen RM, Golden EJ, Obbard RW. Metrics for interpreting the microstructure of sea ice using X-ray micro-computed tomography. *Cold Regions Science and Technology*. 2017 Jun; 138: 24–35.

57 Wren SN, Donaldson DJ. Exclusion of nitrate to the air–ice interface during freezing. *Journal of Physical Chemistry Letters*. 2011 Jul; 2: 1967–1971.

58 Marrocco HA, Michelsen RRH. Nitrate concentration near the surface of frozen aqueous solutions. *Journal of Physical Chemistry B*. 2014 Dec; 118: 14929–14941.

59 Walker RL, Searles K, Willard JA, Michelsen RRH. Total reflection infrared spectroscopy of water-ice and frozen aqueous NaCl solutions. *Journal of Chemical Physics*. 2013 Dec; 139, 244703.

60 Morenz KJ, Donaldson DJ. Chemical morphology of frozen mixed nitrate–salt solutions. *Journal of Physical Chemistry A*. 2017 Mar; 121: 2166−2171.

ToC figure: